

Investigation on the Implementation of Exponential Rate Reaching Law on Parabolic Dish Antenna System

James Nantim¹, A. Mohammed², A. A. Sadiq³, D. M. Nazif⁴

^{1,2,3}Abubakar Tafawa Balewa University Bauchi Bauchi State, Nigeria

⁴Federal Polytechnic Bauchi Bauchi State, Nigeria

jamesbravo.nj@gmail.com; inunugoloma@yahoo.com

Article Info:

Submitted:	Revised:	Accepted:	Published:
Jan 14, 2025	Jan 29, 2025	Feb 10, 2025	Feb 15, 2025

Abstract

Parabolic antennas are crucial in applications like satellite communication, radar systems, and radio astronomy for precise pointing and tracking capabilities. The research aims to create a reliable Exponential Rate Reaching Law-based Proportional-Integral-Derivative (ERPID) controller for a Parabolic Dish Antenna System, overcoming challenges like nonlinearities and wind disturbances. The study integrates the parabolic dish antenna model with PID and ERPID control, evaluating their performances under wind disturbances through simulations. In undisturbed conditions, the antenna system without a controller shows a slow rise time (7.5717 seconds) and extended settling time (9.8105 seconds). When a disturbance is introduced, the system becomes highly unstable with a rapid rise time (0.1047 seconds) and extreme overshoot (657%), demonstrating the need for a controller to manage disturbances. When PID was introduced without Disturbance, the PID controller significantly improved the response. The rise time decreases to 1.4896 seconds, with a settling time of 5.2740 seconds. An overshoot of 9.63% indicates a controlled and responsive system. With Disturbance, the system

maintains stability with a rise time of 1.4977 seconds, though the settling time increases slightly to 9.6556 seconds. Overshoot is kept minimal at 7.9%, showcasing the PID controller's ability to handle disturbances effectively. Without Disturbance, the ERPID controller demonstrates a slower rise time (2.8663 seconds) than the PID, with a comparable settling time of 5.2298 seconds. Overshoot is minimized to 7.66%, indicating high stability and controlled precision. With Disturbance, the ERPID controller maintains a gradual response with a rise time of 2.9832 seconds and a settling time of 6.4649 seconds. The overshoot is further reduced to 6.04%, reflecting robustness against external factors and controlled performance under disturbance. The research revealed that the ERPID controller, despite improving system performance, is more effective for high-precision applications like satellite communication due to its enhanced stability and reduced overshoot.

Keywords: Parabolic Antenna, PID, ERPID, Dryden Disturbance

INTRODUCTION

Antenna systems, first introduced in 1912 by the U.S. Navy, are utilized in various areas like spacecraft, ground communications, and maritime systems for transmitting or receiving signals (Riel et al., 2019). Multi-axis systems with azimuth and elevation gimbals are versatile and robust, used in signals, robotics, weapons systems, optics, and images, particularly in space (Gregory, 2013).

Communication satellites are crucial, but on-orbit systems struggle to meet user demands. Enhancing antenna communications can increase usage and reduce satellites, but this is often impossible or costly due to geosynchronous orbit (Li et al., 2019). Improving flight software can enhance communication satellite coverage by reducing gimbal maneuver time. However, testing software modifications in orbit is not always feasible, so a lab-based system is recommended for evaluation (Li et al., 2019).

A parabolic antenna directs radio waves using a parabolic reflector, used in satellite communication, radar systems, and radio astronomy due to its high gain and directional attributes (Ahlawat et al., 2019). The performance of these antennas is significantly influenced by the effectiveness of their control mechanisms, which must be in the line of sight for continuous and smooth operation (Choubey et al., 2023). Positioning accuracy is crucial as deviations can cause signal loss or weakening, affecting the overall performance

of the communication system (Ahmed et al., 2014, 2015; Ahmed & Noor, 2015). The increasing demand for higher data rates and improved communication capabilities necessitates control systems to optimize the parabolic antenna's orientation and alignment performance.

Mechanical disturbances can cause signal loss or weakness in home TV antennas, even on rooftops for better signal reception, affecting television channels (Alkhalifa, 2016). Manual readjustment is challenging, particularly for larger antennas like telescopes due to their weight or smaller antennas with limited precision (Yadav & Sharma, 2016).

Outdoor antennas face torque disturbances like wind pressure and gusts, requiring control systems to maintain the correct position, azimuth, and elevation angles for the pointing direction (Sakr & Hassan, 2023).

The Reaching Law-based PID controller is a widely used industrial control strategy, utilizing a specific algorithm to determine control output. This method ensures a finite time convergence to the set point, offering faster response times, improved stability, robustness to disturbances, and reduced overshoot. It is commonly used in motor control, process control, robotics, and power systems.

Maintaining parabolic antennas at the line of sight ensures continuous and reliable communications, with increased accuracy due to increased operation requirements and system size (Karacal, 2019). Large telescope and antenna aiming accuracy are crucial for satellite communication, defense, and astronomy, while conventional PID controllers struggle with nonlinearities and wind disturbances (Jonathan et al., 2020). This research aims to develop a reliable control system using Reaching Law-Based PID, reduce obstacles, and improve aiming accuracy.

Antenna Positioning System

Numerous literature exists on the Antenna control system. Some of these works are discussed as under.

Jonathan et al., (2020) designed to improve the Performance Response of Mobile Satellite Dish Antenna Network within Nigeria. The paper enhances Nigeria's mobile satellite dish antenna network performance by addressing time delay variability and ensuring accurate positioning. Simulations show a stable, robust, efficient system with a more efficient time delay handling capacity.

Chen et al., (2022) worked on an Improved Radio Pointing Model for SHARC II of the Caltech Submillimeter Observatory Telescope. The research aims to enhance the radio pointing model of the Submillimeter High Angular Resolution Camera II (SHARC II) at the Caltech Submillimeter Observatory (CSO) telescope using three structural reconstruction methods. The reconstructed model improves pointing error accuracy and is effective for detecting radiation near 1 mm. The model will be continuously updated based on new data and techniques.

Reddy et al., (2022) worked on the Effects of an Integrated Fuzzy Logic PID Controller on a Satellite Antenna Tracking System. The study explores fuzzy control techniques in satellite systems for mobile antenna tracking, recommending stabilized antennas and fuzzy regulators for improved phase and bandwidth, and comparing them with conventional controllers.

Singh & Pal, (2019) utilized Genetic Algorithms (GA) for optimizing feed positioning in wideband beamforming of parabolic antennas. Their study aimed at achieving desired gain and pattern characteristics by evolving optimal feed configurations. Experimental validation highlighted GA's effectiveness in antenna optimization, with limitations in computational expense and practical deployment challenges in real-world environments.

Moon et al., (2019) designed a Phased Array Shaped-Beam Satellite Antenna with Boosted-Beam Control. The communication introduces a beamforming shaped-beam satellite antenna for Korea's southern and northern regions, featuring 19 radiation elements, a boosted-beam control panel, and 19 horn arrays. It measures radiation patterns and extracts IRA performance for uniform beam operation.

Shehzad et al., (2023) focused on a Neuro-fuzzy system-based proportional derivative gain optimized attitude control of CubeSat under LEO perturbations. The Nano CubeSat faces attitude stabilization challenges due to its limited capacity, weight, energy, and volume. An artificial neural network, ANFIS-PD, is developed to control angular velocity and quaternions, achieving minimal errors and rapid stability within 20 seconds.

Eze et al., (2021) proposed a PID-tuned compensator for DC servomotor-based antenna positioning, aiming to reduce rise time and maintain stability against disturbances. The study found significant improvements in performance metrics like rise time and

settling time under zero disturbance conditions, but optimal performance requires complex tuning of PID parameters.

Research on PID control for parabolic dish antenna systems aims to enhance tracking performance and disturbance rejection. Reaching law controllers can reduce challenges like sensor noise and wind disturbances, improving positioning accuracy and response times.

MATERIALS AND METHODS

Dynamics of the Parabolic Antenna

The control system for parabolic antennas is a complex architecture centered around the Antenna Controller Unit (ACU). This unit processes user inputs and sensor feedback to generate commands for motor drives for azimuth and elevation adjustments, utilizing real-time data from encoders and inclinometers (Uthman, 2019).

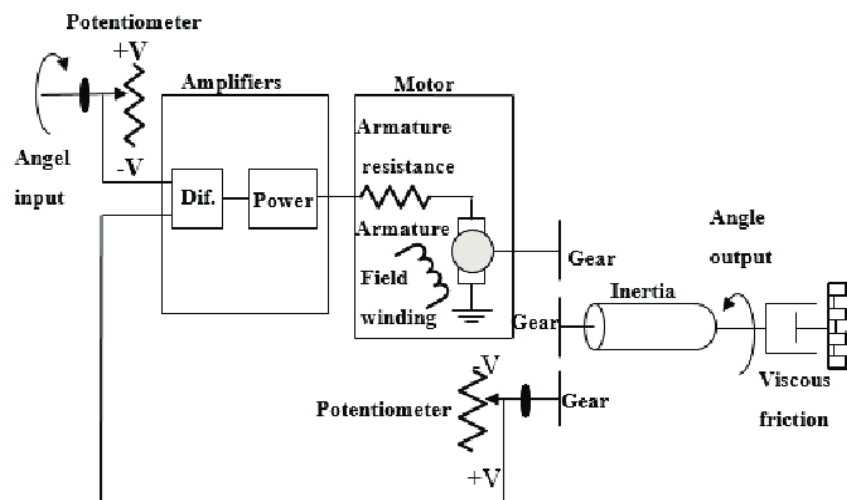


Figure 1: Schematic Diagram of the Parabolic Antenna Control System (Nise, 2015).

PID controllers are crucial for accurate pointing and tracking of parabolic antennas. They integrate target coordinates, environmental variables, and sensor feedback, employing various tracking strategies and safety features to ensure optimal performance across various operational scenarios (Riel et al., 2019).

A more detailed schematic (Figure 1) and block diagram (Figure 2) show a space antenna position control system.

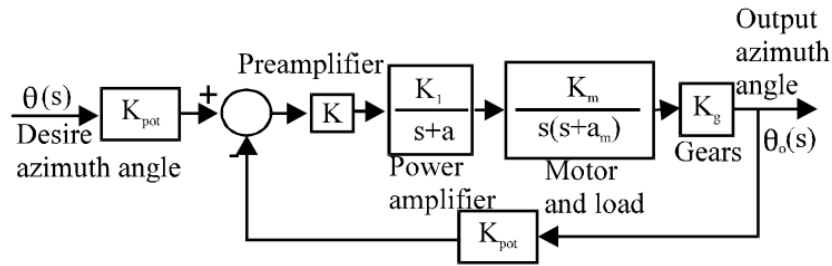


Figure 2: Block Diagram of the Parabolic Antenna Control System (Nise, 2015).

Table 1: Definition of Terms in Antenna Subsystems (Nise, 2015).

Subsystem	Input	Output
Input potentiometer	Angular rotation from a user, $\theta_i(t)$	Voltage to preamp, $v_i(t)$
Preamp	Voltage from potentiometers, $v_e(t) = v_i(t) - v_o(t)$	Voltage to power amp, $v_p(t)$
Power amp	Voltage from preamp, $v_p(t)$	Voltage to motor, $e_a(t)$
Motor	Voltage from power amp, $e_a(t)$	Angular rotation to load, $\theta_o(t)$
Output potentiometer	Angular rotation from load, $\theta_o(t)$	Voltage to preamp, $v_o(t)$

The antenna's hardware, software, and physical structure significantly impact pointing precision, necessitating a balance between accuracy and the required pointing-error budget (Ahlawat et al., 2019).

The purpose of this system is to have the azimuth angle output of the antenna, $\theta_o(t)$, following the input angle of the potentiometer, $\theta_i(t)$.

The system converts input angular displacement into voltage and output voltage through a potentiometer, with a differential amplifier checking the difference and signal and power amplifiers boosting the difference (Nise, 2015). The system drives the motor to zero when the input and output do not match, with a larger input voltage causing faster motor turning (Nise, 2015). This system uses a fixed-field DC servo motor. The antenna position system comprises five subsystems with corresponding transfer functions, as illustrated in Table 2, which outlines all variables utilized in the system (Nise, 2015).

Table 2: Schematic Parameters used in the antenna position system (Nise, 2015).

Parameter	Meaning	Value
V	Voltage across Potentiometer [Volts]	10
N	Turns of potentiometer	1
K	Preamplifier gain	1
K ₁	Power Amplifier gain	100
A	Power Amplifier pole	100
R _a	Motor Resistance [ohms]	5
J _a	Motor Inertial constant [kg-m ²]	0.05
D _a	Motor Dampening constant [N-m s/rad]	0.01
K _b	Back EMF constant [V-s/rad]	1
K _t	Motor Torque constant [N-m/A]	1
N ₁	Gear teeth	50
N ₂	Gear teeth	250
N ₃	Gear teeth	250
J _L	Load inertial constant [kg-m ²]	5
D _L	Load dampening constant [N-m s/rad]	3

The parameters used in modeling the antenna positioning system are given in Table 2.

Input and Output Potentiometer

Neglecting the dynamics of the input and output potentiometers shows the relationship between output voltage and input angular displacement. The potentiometer's block diagram is obtained from Figure 2. The transfer function is given in Equation 1.

$$\frac{V_i(s)}{\theta_i(s)} = K_{pot_i} \quad (1)$$

$$K_{pot_i} = \frac{V}{N\pi} = \frac{10}{1 \times \pi} = 3.18$$

Where $V_i(s)$ Is the voltage from the input potentiometer [V]; $i_i(s)$ is the input angle [rad]; K_{pot} is the potentiometer gain; N is the turns of the potentiometer

Preamplifier

The preamplifier amplifies input signal voltage for power amplifier input, with a specified gain for desired output, modeled by a design engineer. The resulting equation therefore is quite simple, as shown in Equation 2.

$$\frac{V_p(s)}{V_e(s)} = K \quad (2)$$

$V_p(s)$ is the output voltage of the preamplifier [V]; $V_e(s)$ is the voltage after the summation [V]; K is the preamplifier gain

Power Amplifier

The power amplifier converts the preamplifier's output voltage into motor-usable voltage, as specified in the design schematic and block diagram. Also, the values of K_1 and a in the transfer function are given in the configuration data shown in Table 2 above.

$$\begin{aligned} \frac{E_a(s)}{V_p(s)} &= \frac{K_1}{s+a} \\ &= \frac{100}{s+100} \end{aligned} \quad (3)$$

Where $E_a(s)$ is the output voltage of the power amplifier [V]; $V_p(s)$ is the input voltage of the power amplifier from the preamplifier [V]; K_1 is the power amplifier gain; a is the power amplifier pole

Motor and Load

The Power Amplifier, motor, gears, load, antenna, and transfer function must be considered for the mechanical system's transfer function, assumed to be an armature-controlled DC servo motor with a fixed field.

To derive the transfer function of the subsystem one must find Kirchoff's Voltage Law (KVL) equation relating the input voltage to the motor to the output position of the armature (Zhang et al., 2024). Figure 3 shows the general circuit of a motor.

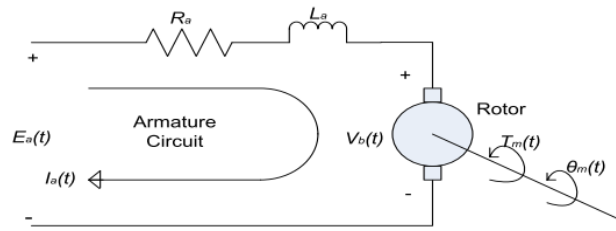


Figure 3: Circuit of a motor (Nise, 2015).

The KVL equation, focusing on input voltage, should be replaced with the equivalent Torque term in equation 5, as we lack information on input current. Definitions of parameters are given in Table 2.

$$R_a I_a(s) + L_a s I_a(s) + V_b(s) = E_a(s) \tag{4}$$

$$T_m(s) = K_t I_a(s)$$

$$I_a(s) = \frac{T_m(s)}{K_t} \tag{5}$$

Where R is the motor resistance [ohms]; I_a is the circuit current [A]; L_a is the motor inductance [H]; $V_b(s)$ is the voltage across the rotor (back EMF) [V]; $E_a(s)$ is the voltage across the motor [V]; $T_m(s)$ is the motor torque [N.m]; K_t is the motor torque constant [N-m/A]

The equation lacks the current term and motor torque, which can be replaced with torque, speed, position, inertia, and dampening, and back EMF term, V_b , to create a transfer function. These are both shown in equations 6 and 7.

$$V_b(s) = K_b s \theta_m(s) \tag{6}$$

$$T_m(s) = (J s^2 + D_m s) \theta_m(s) \tag{7}$$

Where K_b is the back EMF constant [V-s/rad]; $\theta_m(s)$ is the angle of rotation of the rotor [rad]; J is the inertial constant [Kg-m²]; D_m is the dampening constant [N-m s/rad].

Thus, replacing the corresponding variables with their equivalents in equation 2.4, and simplifying creates equation 8.

$$\frac{(J s^2 + D_m s)(R_a + L_a s) \theta_m(s)}{K_t} + K_b s \theta_m(s) = E_a(s) \tag{8}$$

This is making use of the assumption that this is a fixed field motor, which makes K_b and K_t equal. Both of these values are given; for configuration two in Table 2, they are 1. Then pulling

$\theta_m(s)$ to the outside yields equation 9.

$$\left[\frac{(Js^2 + D_m s)(R_a + L_a s) \theta_m(s) + K_b K_t s}{K_t} \right] \theta_m(s) = E_a(s) \quad (9)$$

The definitions of terms are given in Table 2 and assuming that $R_a \gg L_a$ one can further simplify to equation 10.

$$\frac{\theta_m(s)}{E_a(s)} = \frac{\frac{K_t}{J R_a}}{s \left(s + \frac{D_m R_a + K_b K_t}{J R_a} \right)} \quad (10)$$

The damping and inertial components of the system are connected to the motor through a set of gears. This changes their effective values as seen by the motor and must be compensated for. This can be done using equations 12 and 13. The gear ratios are shown in equation 11.

$$K_g = \frac{N_1}{N_2} = \frac{50}{250} = 0.2 \quad (11)$$

$$J = J_a + J_L (K_g)^2 = 0.05 + 5(0.2)^2 = 0.25 \quad (12)$$

$$D_m = D_a + D_L (K_g)^2 = 0.01 + 3(0.2)^2 = 0.13 \quad (13)$$

Where K_g is gear ratio; N is gear teeth; J_a is the motor inertial constant [$\text{kg}\cdot\text{m}^2$]; J_L is the load inertial constant [$\text{kg}\cdot\text{m}^2$]; D_a is motor dampening constant [$\text{N}\cdot\text{m s/rad}$]; D_L is load dampening constant [$\text{N}\cdot\text{m s/rad}$]

Equation 13 is in the same form as the given transfer function for the motor and load, thus we can relate the variables K_m , and a_m . This, along with their computed values is shown in equations 14 and 15.

$$K_m = \frac{K_t}{J R_a} = \frac{1}{0.25 \times 5} = 0.8 \quad (14)$$

$$a_m = \frac{D_m R_a + K_b K_t}{J R_a} = \frac{0.13 \times 5 + 1 \times 1}{0.25 \times 5} = 1.32 \quad (15)$$

Where K_m is motor and load gain m ; a_m is motor and load pole.

Table 2 values were used to compute the values in the above equations and summarized in Table 3.

Figure 4 shows how to reduce the subsystems of the antenna azimuth position control system to a single, closed-loop transfer function to analyze and design the transient response characteristics.

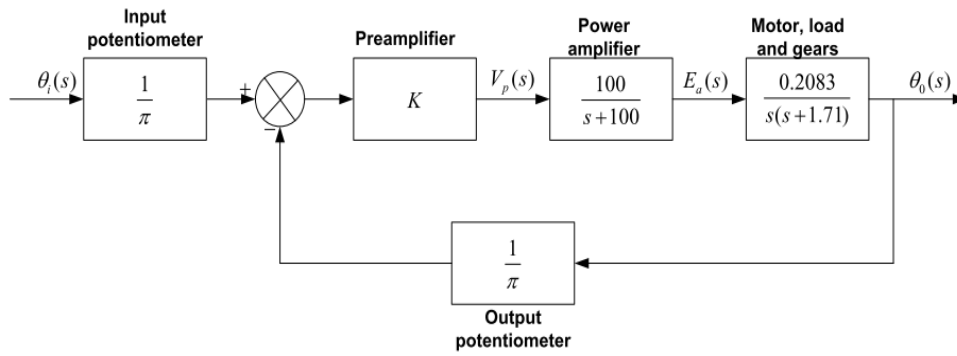


Figure 4: Block Diagram of the antenna position system

Table 3: Block Diagram Parameters used in the antenna position system (Uthman & Sudin, 2018).

Parameter	Meaning	Values
K_{pot}	Potentiometer gain	0.318
K	Preamplifier gain	-
K_1	Power Amplifier gain	100
A	Power Amplifier pole	100
K_m	Motor and load gain	2.083
a_m	Motor and load pole	1.71
K_g	Gear ratio	0.2

The PID Controller

A controller minimizes error between measured process variables and reference, providing feedback and predicting futures. Automatic controllers compare the output with the desired value, while PID controllers offer simplicity, low maintenance, effectiveness, stability, and reliability. Figure 5 explains the PID controller.

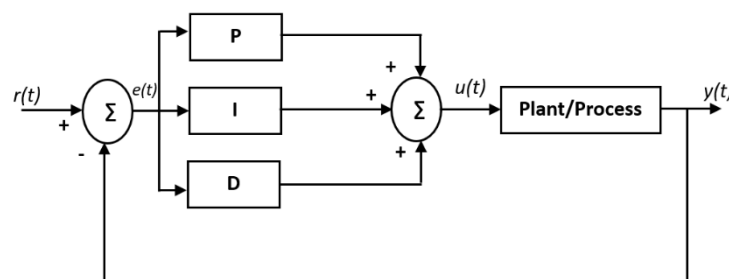


Figure 5: PID Controller

An automatic controller detects and amplifies an actuating error signal, feeding it to an electric motor, ensuring the output of the plant approaches the reference input signal. (Bankole, 2022; Mou & Wu, 2020). A sensor converts the output variable to a suitable unit, comparing it to the reference input, while the controller's set point must be converted to the same units as the feedback signal.

The PID Controller consists of Proportional, Integral, and Derivative components, commonly referred to as P-controllers, PI-controllers, or PD-controllers, which can be modified by removing unnecessary components.

The PID controller calculates the tracking error $e(t)$ and its gains K_p , K_i , and K_D , which together form the control action u , as shown in the following expression:

$$u(t) = K_p e(t) + K_i \int e(t) dt + K_D \frac{de}{dt} \quad (16)$$

where;

K_p = proportional gain, K_i = integral gain, K_d = derivative gain, $e(t)$ = error at the current time, and t = integration variable.

Reaching Law-based PID (ERPID) Controller

The ERPID controller integrates traditional PID control with the reaching law approach, utilizing the exponential rate-reaching law for faster convergence, reduced chattering, and enhanced robustness (Ji et al., 2022). The exponential rate reaching law is represented in equation 17 and the ERPID control signal, $u(t)$, is represented in equation 18.

$$\dot{s} = \eta \operatorname{sign}(s(t)) - ks \quad (17)$$

$$u(t) = K_p e(t) + K_i \int e(t) dt + K_d \frac{de(t)}{dt} + \eta \operatorname{sign}(s(t)) - ks \quad (18)$$

Where: $e(t)$ is the position error, defined as $e(t) = r(t) - \theta(t)$; K is the reaching law gain, which determines the convergence rate of the position error.

The reaching law term, $\eta \times \operatorname{sign}(s(t))$, ensures that the position error converges to zero in finite time, as per the reaching law principle.

H. Disturbance

Wind disturbance significantly impacts antenna positioning control, affecting precise pointing accuracy and causing unwanted movements and deviation from the target in parabolic dish antennas (Chandra et al., 2021; Wajirakumara, 2021).

This research examines the effectiveness of the Dryden wind turbulence model in accurately modeling wind disturbances, and assessing their robustness based on historical data or assumed scenarios (Harris, 2020).

The Dryden model characterizes wind as a first-order system responding to random inputs, with the wind speed $V_{wind}(t)$ modeled. (Tan *et al.*, 2020) as:

$$\dot{v}_{wind}(t) = -\frac{1}{L}v_{wind}(t) + W(t) \quad (19)$$

where L is the turbulence scale length (typically around 10–30 meters, depending on the location and height); $W(t)$ is the white noise process representing random wind fluctuations.

In this case, $v_{wind}(t)$ is a stochastic process that varies over time, simulating realistic wind patterns. The resulting torque $T_{wind}(t)$ then becomes:

$$T_{wind}(t) = \frac{1}{2}C_d\rho Av_{wind}(t)^2 \quad (20)$$

where: C_d is the Drag coefficient, a dimensionless factor depending on the antenna's shape and orientation; ρ is the Air density (approximately 1.225 kg/m³ at sea level); A is the Effective surface area of the antenna facing the wind; $v_{wind}(t)$ is the Instantaneous wind speed (m/s).

Figure 6 shows the model implemented using SIMULINK within the MATLAB environment.

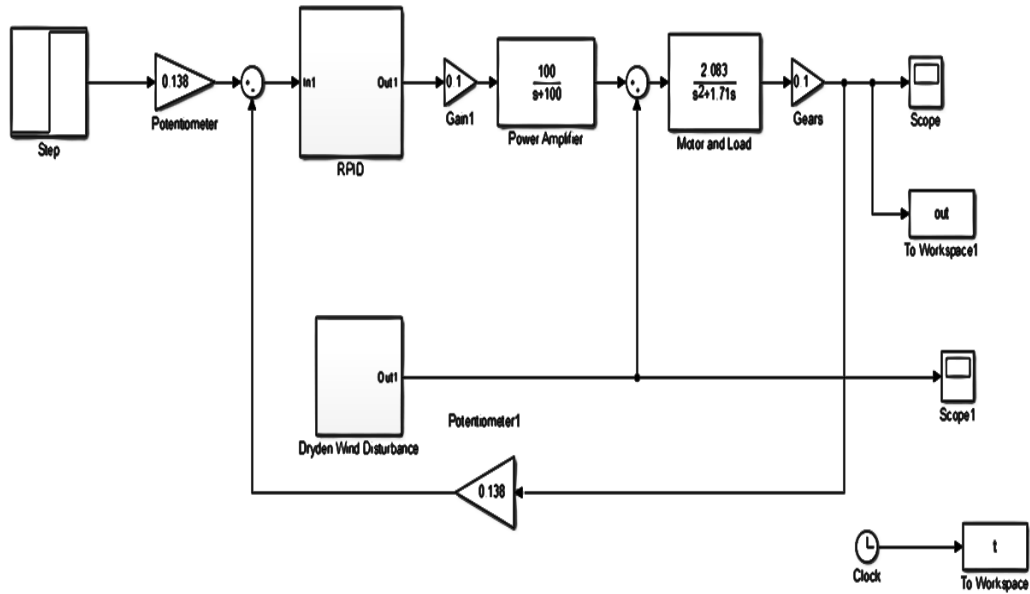


Figure 6: Simulink Block of the Antenna Positioning System

RESULTS AND DISCUSSION

Step Response of the Antenna as a Plant with PID and ERPID without Disturbance

Figure 7 shows the response obtained from the plant without a controller. It also depicts the response with PID and ERPID in the absence of disturbance.

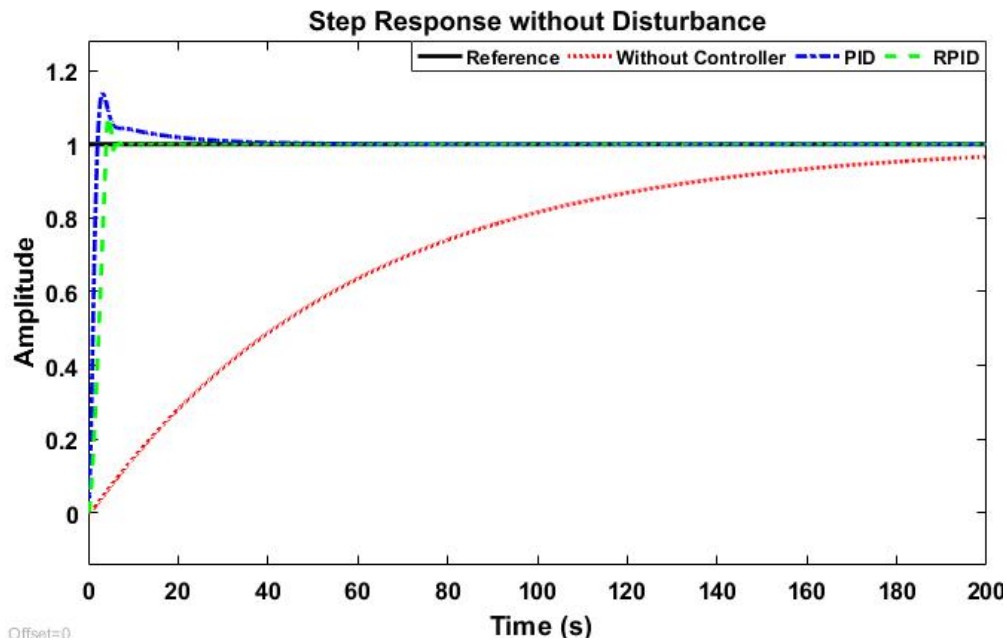


Figure 7: Step Response of the Antenna without Disturbance

Table 4 summarizes the results obtained from Figure 7.

Table 4: Antenna Performance without Disturbance

Parameters	Without Controller	PID	ERPID
Rise Time (s)	7.5717	1.4896	2.8663
Settling Time (s)	9.8105	5.2740	5.2298
Overshoot (%)	0	9.6305	7.6625
Peak Time (s)	10	3.2234	4.5396

Figure 7 shows the results of the antenna positioning system without a controller, with PID and ERPID in the absence of disturbance. Table 4 displays a transient response of time domain parameters, with a rise time of 7.5717 seconds and a settling time of 9.8105 seconds. The system maintains a specified range, with no overshoot, and a peak time of 10 seconds, ensuring stability and precision in tracking applications. The PID controller significantly enhances response stability and speed, reducing rise time to 1.4996 seconds and settling time to 5.2740 seconds, with a minor overshoot of 9.63% indicating a controlled response. The PID controller enhances system responsiveness and stability, achieving accurate positioning without excessive oscillation, resulting in a peak time of 3.2234 seconds. The ERPID controller achieves a slightly slower initial response with a rise time of 2.8663 seconds, but maintains a comparable settling time of 5.2298 seconds, demonstrating effective system stabilization. Its overshoot is modest at 7.66%, and its peak time is 4.5396 seconds.

Step Response of the Antenna as a Plant with PID and ERPID with Disturbance

Figure 8 shows the response obtained from the plant without a controller. It also depicts the response with PID and ERPID in the presence of disturbance.

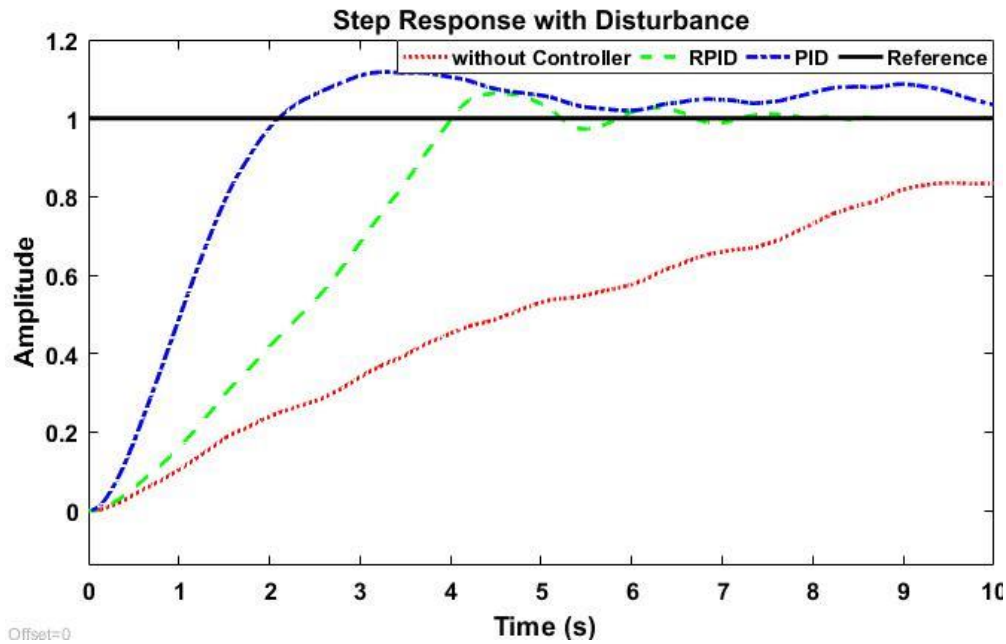


Figure 8: Step Response of the Antenna with Disturbance

Table 5: Antenna Performance with Disturbance

Parameters	Without Controller	PID	ERPID
Rise Time (s)	0.1047	1.4977	2.9832
Settling Time (s)	9.9475	9.6556	6.4649
Overshoot (%)	657.04	7.9046	6.0449
Peak Time (s)	6.0325	3.300	4.5619

The results of the antenna positioning system without a controller but with disturbance reveal a highly unstable response as shown in Figure 8. Table 5 shows the system's transient response without a controller, showing a fast rise time of 0.1047 seconds but an extreme overshoot of 657.04%. The peak time of 6.0325 seconds is far from controlled behavior, and the settling time of 9.9475 seconds suggests a need for a controller for smoother positioning. With the PID controller in place, the antenna positioning system maintains stable performance despite disturbances, with a rise time of 1.4977 seconds and a settling time of 9.6556 seconds. The system maintains a low overshoot of 7.90% and a peak time of 3.30 seconds. The ERPID controller maintains system stability despite disturbances, with a gradual rise time of 2.9832 seconds, a short settling time of 6.4649 seconds, a low overshoot of 6.04%, and a smooth peak time of 4.5619 seconds. The

ERPID controller exhibits resilience to disturbance, maintaining accuracy and control with minimal performance trade-offs compared to an undisturbed scenario.

CONCLUSION

This study aims to apply the ERPID Controller for the Parabolic Dish Antenna System for improved performance. The following conclusions can be made at the end of this research work. The results of the control scheme using the ERPID controller and the PID controller were compared. PID and ERPID controllers enhance antenna positioning system performance, with ERPID offering superior stability. Standard PID improves responsiveness, but sensitivity to disturbances increases settling time. The ERPID controller prioritizes stability over speed, achieving minimal overshoot and enhanced robustness to disturbances, offering a balanced approach for applications requiring accuracy under variable conditions.

Future research could involve real-world testing, hardware-in-the-loop testing, machine learning-based tuning, adaptive algorithms, and advanced control methods like Model Predictive Control or Fuzzy-PID to validate disturbance resilience and tracking accuracy.

Acknowledgment

Contributions from my supervisors, lecturers, family, friends, and colleagues are greatly appreciated.

REFERENCES

- Ahlawat, H. D., Ranga Prasad, M. P., & Chauhan, R. P. (2019). Antenna Azimuthal Position Control Using Model Predictive Control. *Proceedings of 2019 3rd IEEE International Conference on Electrical, Computer and Communication Technologies, ICECCT 2019*, 1–6. <https://doi.org/10.1109/ICECCT.2019.8869043>
- Ahmed, M., Anene, E. C., Jiya, J. D., & Bakare, G. A. (2015). Optimal Design of Controller for Antenna Control Using ACO Approach. *Australian Journal of Basic and Applied Sciences*, 9(27), 209–213.
- Ahmed, M., Bahari, S., Noor, M., Khair, M., Hassan, B., Bt, A., & Soh, C. (2014). A Review of Strategies for Parabolic Antenna Control A Review of Strategies for Parabolic. *Australian Journal of Basic and Applied Sciences*, 8(7), 135–148. www.ajbasweb.com
- Ahmed, M., & Noor, S. B. B. M. (2015). Fuzzy control of parabolic antenna with backlash compensation. *AIP Conference Proceedings*, 1660, 1–8.

<https://doi.org/10.1063/1.4915806>

- Alkhalifa, A. A. O. M. (2016). *Antenna Position Control System, Simulation and Real-time Study*. National Institute of Technology Rourkela.
- Bankole, A. T. (2022). *A Novel Hybrid Proportional Derivative / H-infinity Controller Design for Improved Trajectory Tracking of a Two-Link Robot Arm*.
- Chandra, M., Kumar, S., Chattopadhyaya, S., Chatterjee, S., & Kumar, P. (2021). A review on developments of deployable membrane-based reflector antennas. *Advances in Space Research*, 68(9), 3749–3764. <https://doi.org/10.1016/j.asr.2021.06.051>
- Chen, W., Wang, Z., & Zhou, X. (2022). An Improved Radio Pointing Model for SHARC II of the Caltech Submillimeter Observatory Telescope. *Publications of the Astronomical Society of the Pacific*, 134(1040), 1–20. <https://doi.org/10.1088/1538-3873/ac94f7>
- Eze, P. C., Ugoh, C. A., & Inaibo, D. S. (2021). Positioning Control of DC Servomotor-Based Antenna Using PID Tuned Compensator. *Journal of Engineering Sciences*, 8(1), E9–E16. [https://doi.org/10.21272/jes.2021.8\(1\).e2](https://doi.org/10.21272/jes.2021.8(1).e2)
- Gregory, M. C. (2013). *Design and prototyping of a Satellite Antenna Slew Testbed*. Naval Postgraduate School Monterey, California.
- Harris, J. L. (2020). *Characterization and Sensitivity Analysis of 6 Meter Cassegrain Antenna*. Air Force Institute of Technology, Wright-Patterson Air Force Base, Ohio.
- Ji, P., Li, C., & Ma, F. (2022). Sliding Mode Control of Manipulator Based on Improved Reaching Law and Sliding Surface. *Mathematics*, 10(11). <https://doi.org/10.3390/math10111935>
- Jonathan, Agwah, B. C., & Okoronkwo, E. A. (2020). Improving the Performance Response of Mobile Satellite Dish Antenna Network within Nigeria. *Journal of Electrical Engineering, Electronics, Control and Computer Science-JEEECCS*, 6(21), 25–30.
- Karacal, I. (2019). Design, Modeling and Control of a SATCOM on-the-move Antenna Terminal. In *Sustainability (Switzerland)* (Vol. 11, Issue 1). http://scioteca.caf.com/bitstream/handle/123456789/1091/RED2017-Eng-8ene.pdf?sequence=12&isAllowed=y%0Ahttp://dx.doi.org/10.1016/j.regsciurbeco.2008.06.005%0Ahttps://www.researchgate.net/publication/305320484_SYSTEM_PEMBETUNGAN_TERPUSAT_STRATEGI_MELESTARI
- Li, L., Shi, R., Zhang, X., Ma, J., & Zhang, J. (2019). Design of Motion Controller for Satellite-Borne Data Transmission Antenna. *Hindawi International Journal of Aerospace Engineering*, 2019(6030761), 1–11. <https://doi.org/10.1155/2019/6030761>
- Moon, S. M., Yun, S., Yom, I. B., & Lee, H. L. (2019). Phased Array Shaped-Beam Satellite Antenna with Boosted-Beam Control. *IEEE Transactions on Antennas and Propagation*, 67(12), 7633–7636. <https://doi.org/10.1109/TAP.2019.2930129>
- Mou, F., & Wu, D. (2020). *Active disturbance rejection sliding mode control for robot manipulation*. 1(1), 67–85. <https://doi.org/10.1108/JIMSE-06-2020-0004>
- Nise, N. S. (2015). *Control Systems Engineering* (Weley (ed.); 7Th ed., Vol. 7). John Weley & Sons.
- Reddy, R. O., Kautish, S., Reddy, V. P., Yadav, N. S., Alanazi, M. M., & Mohamed, A. W. (2022). Effects of Integrated Fuzzy Logic PID Controller on Satellite Antenna Tracking System. *Computational Intelligence and Neuroscience*, 2022(7417298), 1–11. <https://doi.org/10.1155/2022/7417298>

- Riel, T., Sinn, A., Schwaer, C., Ploner, M., & Schitter, G. (2019). Iterative trajectory learning for highly accurate optical satellite tracking systems. *Acta Astronautica*, 164(November 2019), 121–129. <https://doi.org/10.1016/j.actaastro.2019.07.012>
- Sakr, M. E. S. M., & Hassan, M. A. M. (2023). Satellite Tracking Control System Using Optimal Variable Coefficients Controllers Based on Evolutionary Optimization Techniques. *El-Cezeri Journal of Science and Engineering*, 10(2), 326–348. <https://doi.org/10.31202/ecjse.1214722>
- Shehzad, M. F., Asghar, A. B., Jaffery, M. H., Naveed, K., & Čonka, Z. (2023). Neuro-fuzzy system based proportional derivative gain optimized attitude control of CubeSat under LEO perturbations. *Heliyon*, 9(10), 1–21. <https://doi.org/10.1016/j.heliyon.2023.e20434>
- Singh, U., & Pal, N. S. (2019). Antenna Azimuth Position Control using Model Reference Adaptive Controller and Self Tuning Controller. *SSRN Electronic Journal*, 1–9. <https://doi.org/10.2139/ssrn.3572811>
- Tan, N. D., Giang, L. N., & Viet, N. D. (2020). Modelling and simulation of a hexapod antenna system for tracking VNREDSAT-1 satellite. *Proceedings - 2020 IEEE International Conference on Environment and Electrical Engineering and 2020 IEEE Industrial and Commercial Power Systems Europe, IEEEIC / I and CPS Europe 2020*, 7281–7455. <https://doi.org/10.1109/IEEEIC/ICPSEurope49358.2020.9160586>
- Uthman, A. (2019). Antenna Azimuth position Control System Using Model Reference Adaptive Control Method Gradient Approach and Stability Approach. *Journal of Engineering and Applied Sciences*, 14(16), 5657–5664.
- Uthman, A., & Sudin, S. (2018). Antenna azimuth position control system using PID controller & state-feedback controller approach. *International Journal of Electrical and Computer Engineering*, 8(3), 1539–1550. <https://doi.org/10.11591/ijece.v8i3.pp1539-1550>
- Wajirakumara, A. (2021). *Simulation of Precise Automatic Radio Frequency Ground Station Tracking For S-Band Satellites* [Luleå University of Technology]. www.diva-portal.org/smash/record.jsf?pid=diva2:1548727
- Yadav, S., & Sharma, V. (2016). Performance Evaluation of Azimuth P Radio Telescope in Matlab/Simulink using P and PD Controllers. *Research Journal of Engineering Sciences*, 5(11), 1–8.
- Zhang, Y., Zhang, M., Liu, C., Feng, Z., & Xu, Y. (2024). Reliability enhancement of state of health assessment model of lithium-ion battery considering the uncertainty with quantile distribution of deep features. *Reliability Engineering and System Safety*, 245(February), 110002. <https://doi.org/10.1016/j.ress.2024.110002>